Experimental Identification of Generalized Proportional Viscous Damping Matrix

S. Adhikari[1]
Department of Aerospace Engineering,
University of Bristol,
Bristol BS8 1TR, UK
e-mail: s.adhikari@bristol.ac.uk

A. Srikantha Phani
Department of Engineering,
University of Cambridge,
Cambridge CB2 1PZ, UK
e-mail: skpa2@eng.cam.ac.uk

A simple and easy-to-implement algorithm to identify a generalized proportional viscous damping matrix is developed in this work. The chief advantage of the proposed technique is that only a single drive-point frequency response function (FRF) measurement is needed. Such FRFs are routinely measured using the standard techniques of an experimental modal analysis, such as impulse test. The practical utility of the proposed identification scheme is illustrated on three representative structures: (1) a free-free beam in flexural vibration, (2) a quasiperiodic three-cantilever structure made by inserting slots in a plate in out-of-plane flexural vibration, and (3) a point-coupled-beam system. The finite element method is used to obtain the mass and stiffness matrices for each system, and the damping matrix is fitted to a measured variation of the damping (modal damping factors) with the natural frequency of vibration. The fitted viscous damping matrix does accommodate for any smooth variation of damping with frequency, as opposed to the conventional proportional damping matrix. It is concluded that a more generalized viscous damping matrix, allowing for a smooth variation of damping as a function of frequency, can be accommodated within the framework of standard finite element modeling and vibration analysis of linear systems. [DOI: 10.1115/1.2980400]

1 Introduction

All structures exhibit damping when subjected to vibrations. Steady state harmonic vibration can be viewed as a cyclical exchange of energy from elastic potential energy to kinetic energy. Such an energy exchange mechanism is not completely efficient in the sense that the structure would lose some mechanical energy in each cycle. The energy is converted into other thermodynamically irreversible forms such as heat. The specific ways in which vibration energy is dissipated are dependent on the underlying physical mechanisms, which are numerous, complex, and often nonlinear [1,2]. For example, modeling damping due to friction at joints in a typical built-up structure such as an aircraft wing or an automotive body is beyond the reach of the current state of the art [3]. Considerable difficulties arise when damping models other than viscous are considered [4]. Given the complexity in detail, it is not surprising that fairly simple *viscous* damping models that account for the overall amount of energy loss have gained wide popularity among engineers. Proportional or Rayleigh damping is one such engineering model. The origins of this model can be traced to the works of Lord Rayleigh [5] in 1877.

The equation of motion of a viscously damped system is expressed by

$$\mathbf{M}\ddot{\mathbf{q}}(t) + \mathbf{C}\dot{\mathbf{q}}(t) + \mathbf{K}\mathbf{q}(t) = \mathbf{f}(t) \tag{1}$$

where $\mathbf{M}$, $\mathbf{C}$, and $\mathbf{K}$ are, respectively, the $N \times N$ mass, viscous damping, and stiffness matrices, $\mathbf{f}(t)$ is the applied forcing function, and $\mathbf{q}(t)$ is the dynamic displacement response. If the system were undamped, then Eq. (1) could be solved very efficiently using the techniques of modal analysis [6–11]. In this case the undamped modes, also known as classical normal modes, satisfy an orthogonality relationship with respect to the mass and stiffness matrices, as expressed by

$$\mathbf{\Phi}^T\mathbf{M}\mathbf{\Phi} = \mathbf{I} \tag{2}$$

$$\mathbf{\Phi}^T\mathbf{K}\mathbf{\Phi} = \mathbf{\Omega}^2 \tag{3}$$

Here modes are normalized according to Eq. (2) and

$$\mathbf{\Omega} = \mathrm{diag}[\omega_1, \omega_2, \ldots, \omega_N] \in \mathbb{R}^{N\times N} \tag{4}$$

$$\mathbf{\Phi} = [\boldsymbol{\phi}_1, \boldsymbol{\phi}_2, \ldots, \boldsymbol{\phi}_N] \in \mathbb{R}^{N\times N} \tag{5}$$

The eigenvalues are arranged such that $\omega_1 < \omega_2 < \omega_3, \ldots, < \omega_k$. The above "modal" analysis significantly simplifies the dynamic analysis because complex multiple-degree-of-freedom (MDOF) systems can be effectively treated as a collection of single-degree-of-freedom oscillators.

To include dissipation in the modal analysis of nonconservative systems, which most of the real structures are, it is convenient to assume proportional damping: a special type of viscous damping. The proportional damping model expresses the damping matrix as a linear combination of the mass and stiffness matrices, that is,

$$\mathbf{C} = \alpha_1\mathbf{M} + \alpha_2\mathbf{K} \tag{6}$$

where α_1 and α_2 are real scalars. This damping model is also known as "Rayleigh damping" or "classical damping." Modes of classically damped systems preserve the simplicity of the real normal modes as in the undamped case and, hence, the justification for a proportional damping model. Caughey and O'Kelly [12] derived the condition that the system matrices must satisfy so that viscously damped linear systems possess classical normal modes. They proved that the series representation of damping

$$\mathbf{C} = \mathbf{M}\sum_{j=0}^{N-1} \alpha_j(\mathbf{M}^{-1}\mathbf{K})^j \tag{7}$$

is the *necessary and sufficient* condition for the existence of classical normal modes for systems without any repeated roots. If only the first two terms of this series are retained, then we recover the Rayleigh damping in Eq. (6). Later Adhikari [13] proposed a further generalization of proportional damping by which the damping matrix can be expressed in terms of smooth continuous functions involving specially arranged mass and stiffness matrices. In this paper we will discuss an experimental identification of the generalized proportional damping.

[1]Corresponding author.

Contributed by the Technical Committee on Vibration and Sound of ASME for publication in the JOURNAL OF VIBRATION AND ACOUSTICS. Manuscript received July 27, 2006; final manuscript received February 28, 2007; published online January 6, 2009. Assoc. Editor: Jonathan Wickert.

System identification plays a crucial role in the validation of numerical models. In the context of damped multiple-degree-of-freedom linear dynamical systems, the process of system identification involves identification of the mass, damping, and stiffness matrices. While it is possible to obtain the mass and stiffness matrices of a system using the finite element (FE) method, the damping matrix must generally be identified with experimental measurements. Many researches have proposed methods to identify the viscous damping matrix from experimental measurements (see Pilkey and Inman [14] for a survey). These methods can be divided into two broad categories [15]: (a) damping identification from modal testing and analysis [13,16–31] and (b) direct damping identification from the forced response measurements in the frequency or time domain [15,32–39]. The modal method entails estimating the modal parameters, such as natural frequencies, damping ratio, and mode shapes, from the measured transfer functions, and consequently the damping matrix is reconstructed from the estimated modal parameters. Direct methods, on the other hand, bypass the modal parameter extraction step and fit the damping matrix to the measured response. A recent study has classified and compared different viscous damping identification methods [40].

Complex engineering structures, in general, will have nonproportional damping. For a nonproportionally damped system, the equations of motion in the modal coordinates are coupled through the off-diagonal terms of the modal damping matrix (damping matrix transformed into modal basis), and consequently the system possesses complex modes instead of real normal modes. Complex modes can arise for various other reasons also [41], for example, due to the gyroscopic effects, aerodynamic effects, nonlinearity, and experimental noise. Adhikari and Woodhouse [24,25] proposed a few methods to identify damping from experimentally identified complex modes. In spite of a large amount of research, understanding and identification of complex modes are not well developed as real normal modes. The main reasons are as follows [4]:

- By contrast with real normal modes, the "shapes" of complex modes are not generally clear. It appears that unlike the (real) scaling of real normal modes, the (complex) scaling or normalization of complex modes has a significant effect on their geometric appearance. This makes it particularly difficult to experimentally identify complex modes in a consistent manner [42].
- The imaginary parts of the complex modes are usually very small compared to the real parts, especially when the damping is small and the modes are well separated [4]. This makes it difficult to reliably extract complex modes using numerical optimization methods in conjunction with experimentally obtained transfer function residues.
- The phase of complex modes is highly sensitive to experimental errors, ambient conditions, and measurement noise and is often not repeatable in a satisfactory manner [4].

In order to bypass these difficulties, often real normal modes are used in an experimental modal analysis. A detailed analysis on the measurability of complex modes can be found in Ref. [4].

The experimental damping identification method proposed in this paper assumes that the system is effectively proportionally damped so that the complex modes can be neglected. The outline of the paper is as follows. In Sec. 2, the generalized proportional damping is briefly reviewed. The damping identification method using the generalized proportional damping is discussed in Sec. 3. The issues regarding the error propagation associated with the method are discussed in Sec. 4. The proposed damping identification technique is applied to a free-free beam, a quasiperiodic clamped plate with slots, and two coupled beams in Secs. 5–7.

2 Generalized Proportional Damping

2.1 Derivation of the Damping Model. The concept of generalized proportional damping was recently introduced by Adhikari [13]. Here we briefly review the main formulation. Caughey and O'Kelly [12] proved that a damped linear system of form (1) can possess classical normal modes if and only if the system matrices satisfy the relationship $\mathbf{K}\mathbf{M}^{-1}\mathbf{C}=\mathbf{C}\mathbf{M}^{-1}\mathbf{K}$. When the system matrices are non-negative definite, interchanging $\mathbf{M}$, $\mathbf{K}$, and $\mathbf{C}$ successively, we have the following basic theorem:

THEOREM 1. *A viscously damped linear system can possess classical normal modes if and only if at least one of the following conditions is satisfied: (a)* $\mathbf{K}\mathbf{M}^{-1}\mathbf{C}=\mathbf{C}\mathbf{M}^{-1}\mathbf{K}$, *(b)* $\mathbf{M}\mathbf{K}^{-1}\mathbf{C}=\mathbf{C}\mathbf{K}^{-1}\mathbf{M}$, and *(c)* $\mathbf{M}\mathbf{C}^{-1}\mathbf{K}=\mathbf{K}\mathbf{C}^{-1}\mathbf{M}$.

If a system has any of the matrices ($\mathbf{K}$, $\mathbf{M}$, or $\mathbf{C}$) singular then the condition(s) involving that matrix has (have) to be disregarded and the remaining condition(s) has (have) to be used in the above result. The concept of generalized proportional damping was proposed by Adhikari [13] using Theorem 1. Here we briefly review the main points required for further developments.

Consider conditions (a) and (b) of Theorem 1; premultiplying (a) by $\mathbf{M}^{-1}$ and (b) by $\mathbf{K}^{-1}$, one has

$$[\mathbf{M}^{-1}\mathbf{K}][\mathbf{M}^{-1}\mathbf{C}]=[\mathbf{M}^{-1}\mathbf{C}][\mathbf{M}^{-1}\mathbf{K}] \text{ or } \mathbf{A}\mathbf{B}=\mathbf{B}\mathbf{A}$$

$$[\mathbf{K}^{-1}\mathbf{M}][\mathbf{K}^{-1}\mathbf{C}]=[\mathbf{K}^{-1}\mathbf{C}][\mathbf{K}^{-1}\mathbf{M}] \text{ or } \mathbf{A}^{-1}\mathbf{D}=\mathbf{D}\mathbf{A}^{-1} \tag{8}$$

where $\mathbf{A}=\mathbf{M}^{-1}\mathbf{K}$, $\mathbf{B}=\mathbf{M}^{-1}\mathbf{C}$, and $\mathbf{D}=\mathbf{K}^{-1}\mathbf{C}$. The role of this commutative property in classical normal loads is revisited in Ref. [43]. For any two matrices $\mathbf{A}$ and $\mathbf{B}$, if $\mathbf{A}$ commutes with $\mathbf{B}$, $\beta(\mathbf{A})$ also commutes with $\mathbf{B}$, where the real function $\beta(x)$ is smooth and analytic in the neighborhood of all the eigenvalues of $\mathbf{A}$. Thus, in view of the commutative relationships in Eq. (8), the representations like $\mathbf{C}=\mathbf{M}\beta(\mathbf{M}^{-1}\mathbf{K})$ and $\mathbf{C}=\mathbf{K}\beta(\mathbf{K}^{-1}\mathbf{M})$ can be used. The damping matrix can be expressed by adding these two quantities as

$$\mathbf{C}=\mathbf{M}\beta_1(\mathbf{M}^{-1}\mathbf{K})+\mathbf{K}\beta_2(\mathbf{K}^{-1}\mathbf{M}) \tag{9}$$

such that the system possesses classical normal modes. The functions $\beta_1(\cdot)$ and $\beta_2(\cdot)$ should be analytic in the neighborhood of all the eigenvalues of their argument matrices. Moreover, $\beta_i(\cdot)$ should be a mapping from the positive real line to the positive real line, that is, $\beta_i(\cdot):\mathbb{R}^+\to\mathbb{R}^+$ for $\mathbf{C}$ to be positive definite. In spite of this restriction, these functions can have very general forms. The expressions of $\mathbf{C}$ in Eq. (9) gets restricted because of the special nature of the *arguments* in the functions.

Rayleigh's result Eq. (6) can be obtained directly from Eq. (9) as a special case by choosing each matrix function as a real scalar times an identity matrix, that is,

$$\beta_i(\bullet)=\alpha_i\mathbf{I}, \quad i=1,2 \tag{10}$$

The damping matrix expressed in Eq. (9) provides a new way of interpreting the Rayleigh damping or "proportional damping" where the scalar constants α_i associated with $\mathbf{M}$ and $\mathbf{K}$ are replaced by arbitrary matrix functions $\beta_i(\cdot)$ with proper arguments. This kind of damping model is called *generalized proportional damping* [13]. From this discussion we have the following general result:

THEOREM 2. *Viscously damped symmetric positive definite linear systems will have classical normal modes if and only if the damping matrix can be represented by* $\mathbf{C}=\mathbf{M}\beta_1(\mathbf{M}^{-1}\mathbf{K})+\mathbf{K}\beta_2(\mathbf{K}^{-1}\mathbf{M})$, *where* $\beta_1(\cdot)$ *and* $\beta_2(\cdot)$ *are smooth analytic functions in the neighborhood of all the eigenvalues of their argument matrices.*

2.2 The Modal Damping Factors. With Rayleigh's proportional damping in Eq. (6), the modal damping factors have the special form

$$\zeta_j = \frac{1}{2}\left(\frac{\alpha_1}{\omega_j} + \alpha_2 \omega_j\right) \tag{11}$$

Clearly, not all forms of variations of ζ_j with respect to ω_j can be captured using Eq. (11). The motivation of using the generalized proportional damping is the ability to model the frequency variation of the damping factors in a simple manner. Using Eqs. (2) and (3), one obtains

$$\mathbf{M} = \mathbf{\Phi}^{-T}\mathbf{\Phi}^{-1}, \quad \mathbf{K} = \mathbf{\Phi}^{-T}\mathbf{\Omega}^2\mathbf{\Phi}^{-1} \tag{12}$$

$$\mathbf{M}^{-1}\mathbf{K} = \mathbf{\Phi}\mathbf{\Omega}^2\mathbf{\Phi}^{-1} \text{ and } \mathbf{K}^{-1}\mathbf{M} = \mathbf{\Phi}\mathbf{\Omega}^{-2}\mathbf{\Phi}^{-1} \tag{13}$$

Because the functions $\beta_1(\cdot)$ and $\beta_2(\cdot)$ are assumed to be analytic in the neighborhood of all the eigenvalues of $\mathbf{M}^{-1}\mathbf{K}$ and $\mathbf{K}^{-1}\mathbf{M}$ respectively, they can be expressed in polynomial forms using the Taylor series expansion. Following Bellman [44] (Chap. 6), we may obtain

$$\beta_1(\mathbf{M}^{-1}\mathbf{K}) = \mathbf{\Phi}\beta_1(\mathbf{\Omega}^2)\mathbf{\Phi}^{-1} \tag{14}$$

$$\beta_2(\mathbf{K}^{-1}\mathbf{M}) = \mathbf{\Phi}\beta_2(\mathbf{\Omega}^{-2})\mathbf{\Phi}^{-1} \tag{15}$$

Considering Theorem 2 and using Eqs. (12) and (13), we have

$$\begin{aligned}\mathbf{\Phi}^T\mathbf{C}\mathbf{\Phi} &= \mathbf{\Phi}^T[\mathbf{M}\beta_1(\mathbf{M}^{-1}\mathbf{K}) + \mathbf{K}\beta_2(\mathbf{K}^{-1}\mathbf{M})]\mathbf{\Phi} \\ &= \mathbf{\Phi}^T[\mathbf{\Phi}^{-T}\mathbf{\Phi}^{-1}\beta_1(\mathbf{M}^{-1}\mathbf{K}) + \mathbf{\Phi}^{-T}\mathbf{\Omega}^2\mathbf{\Phi}^{-1}\beta_2(\mathbf{K}^{-1}\mathbf{M})]\mathbf{\Phi}\end{aligned} \tag{16}$$

Utilizing Eqs. (14) and (15) and carrying out the matrix multiplications, Eq. (16) reduces to

$$\begin{aligned}\mathbf{\Phi}^T\mathbf{C}\mathbf{\Phi} &= [\mathbf{\Phi}^{-1}\mathbf{\Phi}\beta_1(\mathbf{\Omega}^2)\mathbf{\Phi}^{-1} + \mathbf{\Omega}^2\mathbf{\Phi}^{-1}\mathbf{\Phi}\beta_2(\mathbf{\Omega}^{-2})\mathbf{\Phi}^{-1}]\mathbf{\Phi} \\ &= \beta_1(\mathbf{\Omega}^2) + \mathbf{\Omega}^2\beta_2(\mathbf{\Omega}^{-2})\end{aligned} \tag{17}$$

This equation can be written in terms of the modal damping factors as

$$2\boldsymbol{\zeta}\mathbf{\Omega} = \beta_1(\mathbf{\Omega}^2) + \mathbf{\Omega}^2\beta_2(\mathbf{\Omega}^{-2}) \tag{18}$$

$$\text{or } \boldsymbol{\zeta} = \tfrac{1}{2}[\mathbf{\Omega}^{-1}\beta_1(\mathbf{\Omega}^2) + \mathbf{\Omega}\beta_2(\mathbf{\Omega}^{-2})] \tag{19}$$

or

$$\zeta_j = \frac{1}{2}\frac{\beta_1(\omega_j^2)}{\omega_j} + \frac{1}{2}\omega_j\beta_2(1/\omega_j^2) \tag{20}$$

This analysis shows that using the generalized proportional damping, it is possible to model any variation of the damping factors with respect to the frequency. This is the basis and motivation behind the damping identification method discussed in the next section.

3 Damping Identification Using Generalized Proportional Damping

3.1 Damping Identification in a Single Subsystem. From Eq. (20) it can be observed that for the purpose of damping identification, the function β_2 can be omitted without any loss of generality. The functional variation represented by the second term in Eq. (20) can be accommodated by redefining the function β_1 suitably. To simplify the identification procedure, the damping matrix is therefore expressed by

$$\mathbf{C} = \mathbf{M}f(\mathbf{M}^{-1}\mathbf{K}) \tag{21}$$

Using this simplified expression, the modal damping factors can be obtained as

$$2\zeta_j\omega_j = f(\omega_j^2) \tag{22}$$

$$\text{or } \zeta_j = \frac{1}{2\omega_j}f(\omega_j^2) = \hat{f}(\omega_j) \text{ (say)} \tag{23}$$

The function $\hat{f}(\cdot)$ can be obtained by fitting a continuous function representing the variation of the measured modal damping factors with respect to the natural frequencies. In order to obtain a positive definite identified damping matrix, the function $\hat{f}(\cdot)$ must be a mapping from the positive real line to the positive real line, that is, $\hat{f}(\cdot):\mathbb{R}^+ \to \mathbb{R}^+$. From Eqs. (21) and (22), note that in the argument of $f(\cdot)$, the term ω_j can be replaced by $\sqrt{\mathbf{M}^{-1}\mathbf{K}}$ while obtaining the damping matrix. With the fitted function $\hat{f}(\cdot)$, the damping matrix can be identified using Eq. (23) as

$$2\zeta_j\omega_j = 2\omega_j\hat{f}(\omega_j) \tag{24}$$

$$\text{or } \hat{\mathbf{C}} = 2\mathbf{M}\sqrt{\mathbf{M}^{-1}\mathbf{K}}\hat{f}(\sqrt{\mathbf{M}^{-1}\mathbf{K}}) \tag{25}$$

The damping identification procedure itself does not introduce significant errors as long as the modes are not highly complex. From Eq. (25) it is obvious that the accuracy of the fitted damping matrix depends heavily on the accuracy of the mass and stiffness matrix models. In summary, this identification procedure can be described by the following steps:

1. Measure a suitable transfer function $H_{ij}(\omega)$ by conducting vibration testing.
2. Obtain the undamped natural frequencies ω_j and modal damping factors ζ_j, for example, using the circle-fitting method.
3. Fit a function $\zeta = \hat{f}(\omega):\mathbb{R}^+ \to \mathbb{R}^+$, which represents the variation of ζ_j with respect to ω_j for the range of frequencies considered in the study.
4. Calculate the temporary matrix

$$\mathbf{T} = \sqrt{\mathbf{M}^{-1}\mathbf{K}} \tag{26}$$

5. Obtain the damping matrix using

$$\hat{\mathbf{C}} = 2\mathbf{M}\mathbf{T}\hat{f}(\mathbf{T}) \tag{27}$$

Most of the currently available finite element based modal analysis packages usually offer Rayleigh's proportional damping model or a constant damping factor model. A generalized proportional damping model together with the proposed damping identification technique can be easily incorporated within the existing finite element tools to enhance their damping modeling capabilities without using significant additional resources.

3.2 Damping Identification in Coupled Subsystems. The method proposed in the previous section is ideally suitable for small structures for which "global" measurements can be obtained. For a large complex structure such as an aircraft, neither the global vibration measurements nor the processing of global mass and stiffness matrices in the manner described before are straightforward. However, it is possible to identify the generalized proportional damping models for different components or substructures chosen suitably. For example, to model the damping of an aircraft fuselage, one could fit generalized proportional damping models for all the ribs and panels by testing them separately and then combine the element (or substructure) damping matrices in a way similar to the assembly of the mass and stiffness matrices in the standard finite element method. The overall damping modeling procedure can be described as follows:

1. Divide a structure into m elements/substructures suitable for individual vibration testing.
2. Measure a transfer function $H_{ij}^{(e)}(\omega)$ by conducting vibration testing of the eth element/substructure.

3. Obtain the undamped natural frequencies $\omega_j^{(e)}$ and modal damping factors $\zeta_j^{(e)}$ for the eth element/substructure.
4. Fit a function $\zeta_{(e)}=\hat{f}_{(e)}(\omega):\mathbb{R}^+\rightarrow\mathbb{R}^+$, which represents the variation of damping factors with respect to the frequency for the eth element/substructure.
5. Calculate the matrix $\mathbf{T}_{(e)}=\sqrt{\mathbf{M}_{(e)}^{-1}\mathbf{K}_{(e)}}$.
6. Obtain the element/substructure damping matrix using the fitted proportional damping function as $\hat{\mathbf{C}}_{(e)}=2\mathbf{M}_{(e)}\mathbf{T}_{(e)}\hat{f}_{(e)}\times(\mathbf{T}_{(e)})$.
7. Repeat steps 2–6 for all $e=1,2,\ldots,m$.
8. Obtain the global damping matrix as $\hat{\mathbf{C}}=\Sigma_{e=1}^{m}\hat{\mathbf{C}}_{(e)}$. Here the summation is over the relevant degrees-of-freedom as in the standard finite element method.

It is anticipated that the above procedure would result in a more realistic damping matrix compared to simply using the damping factors arising from global vibration measurements. Using this approach, the damping matrix will be proportional only within an element/substructure level. After the assembly of the element/substructure matrices, the global damping matrix will, in general, be nonproportional. Experimental and numerical works are currently in progress to test this method for large systems.

4 Error Propagation in the Damping Identification Method

In the previous section, the method for damping identification was developed, assuming that the mass and stiffness matrices are known exactly. The presence of modeling errors of some kind is inevitable in any experimental analysis. In this section, the influence of errors in the mass and stiffness matrices on the identified viscous damping matrix is investigated. For detailed discussions on the correlation and updating of the mass and stiffness matrices, we refer the readers to Refs. [6–8,45,46].

Consider that errors in the mass and stiffness matrices are $\mathbf{\Delta M}$ and $\mathbf{\Delta K}$. In reality these errors are random in nature. Here we assume that the symmetric matrices $\mathbf{\Delta M}$ and $\mathbf{\Delta K}$ are small compared to $\mathbf{M}$ and $\mathbf{K}$ so that they only represent a "first-order" effect. Suppose the system matrices are function of a variable θ. Therefore, the identified damping matrix

$$\hat{\mathbf{C}}(\theta)=2\mathbf{M}(\theta)[\mathbf{T}(\theta)\hat{f}(\mathbf{T}(\theta))] \tag{28}$$

where

$$\mathbf{T}(\theta)=\sqrt{\mathbf{M}^{-1}(\theta)\mathbf{K}(\theta)} \tag{29}$$

Differentiating Eq. (28) with respect to θ, we have

$$\frac{\partial\hat{\mathbf{C}}(\theta)}{\partial\theta}=2\frac{\partial\mathbf{M}(\theta)}{\partial\theta}\mathbf{T}(\theta)\hat{f}(\mathbf{T}(\theta))+2\mathbf{M}(\theta)\left[\frac{\partial\mathbf{T}(\theta)}{\partial\theta}\hat{f}(\mathbf{T}(\theta))+\mathbf{T}(\theta)\hat{f}'(\mathbf{T}(\theta))\frac{\partial\mathbf{T}(\theta)}{\partial\theta}\right] \tag{30}$$

where $\hat{f}'(x)=\partial\hat{f}/\partial x$. Differentiating Eq. (29) with respect to θ (see the book by Harville [47], Chap. 15 for matrix differentiation), we have

$$\frac{\partial\mathbf{T}(\theta)}{\partial\theta}=\frac{1}{2}[\mathbf{M}^{-1}(\theta)\mathbf{K}(\theta)]^{-1/2}\left[\mathbf{M}^{-1}(\theta)\frac{\partial\mathbf{M}(\theta)}{\partial\theta}\mathbf{M}^{-1}\mathbf{K}(\theta)+\mathbf{M}^{-1}(\theta)\frac{\partial\mathbf{K}(\theta)}{\partial\theta}\right]=\frac{1}{2}\mathbf{T}^{-1}(\theta)\left[\mathbf{M}^{-1}(\theta)\frac{\partial\mathbf{M}(\theta)}{\partial\theta}\mathbf{T}^2(\theta)+\mathbf{M}^{-1}(\theta)\frac{\partial\mathbf{K}(\theta)}{\partial\theta}\right] \tag{31}$$

Considering that θ as the elements of the matrices and variations are small, we can write $\partial\mathbf{M}(\theta)/\partial\theta\approx\mathbf{\Delta M}$ and $\partial\mathbf{K}(\theta)/\partial\theta\approx\mathbf{\Delta K}$ for all θ. We are interested in calculating $\mathbf{\Delta}\hat{\mathbf{C}}\approx\partial\hat{\mathbf{C}}(\theta)/\partial\theta$. Substituting $\partial\mathbf{T}(\theta)/\partial\theta$ from Eq. (31) into Eq. (30) and simplifying, we have

$$\mathbf{\Delta}\hat{\mathbf{C}}\approx\mathbf{T}[3\hat{f}(\mathbf{T})+\mathbf{T}\hat{f}'(\mathbf{T})]\mathbf{\Delta M}+\mathbf{T}^{-1}[\hat{f}(\mathbf{T})+\mathbf{T}\hat{f}'(\mathbf{T})]\mathbf{\Delta K} \tag{32}$$

This equation shows how the errors in the mass and stiffness matrixces propagate through the damping identification procedure.

Table 1 Material and geometric properties of the beam considered for the experiment

Beam properties	Numerical values
Length (L)	1.00 m
Width (b)	39.0 mm
Thickness (t_h)	5.93 mm
Mass density (ρ)	7800 kg/m^3
Young's modulus (E)	210 GPa
Cross sectional area ($a=bt_h$)	2.3127×10^{-4} m^2
Moment of inertia ($I=1/12bt_h^3$)	6.7772×10^{-10} m^4
Mass per unit length (ρ_l)	1.8039 kg/m
Bending rigidity (EI)	135.5431 Nm^2

5 Damping Identification in a Free-Free Beam

5.1 System Model and Experimental Methodology. A steel beam with a uniform rectangular cross section is considered for the experiment. The physical and geometrical properties of the steel beam are shown in Table 1. For the purpose of this experiment, a double sided glued tape is sandwiched between the beam and a thin aluminum plate. This arrangement is similar to a constrained layer damping (see Ref. [48] for a review on this topic).

The impulse is applied at 11 uniformly spaced locations on the beam. We have tried to simulate the free-free condition for the beam by hanging it using two strings. The two string arrangement for suspending the beam is found to reduce the torsional modes. A schematic diagram of the experimental setup is shown in Fig. 1

The vibration response of the beam is measured using the Polytec™ laser vibrometer. The laser beam, which is targeted at a selected measurement point on the test structure, is reflected and interferes with a reference beam inside the scanning head. Since the surface of the test structure movies in space with a varying velocity due to vibrations, the reflected laser beam will have a frequency that is different from that of the reference beam. This is due to the well known Doppler effect. Measuring this shift in frequency permits the determination of the velocity component of the surface in a direction parallel to the laser beam. The interfered light is processed by the vibrometer controller, which generates an *analog* voltage signal that is proportional to the surface target velocity in the direction parallel to the emitted laser beam. By sampling a reference signal, the laser scanner can be triggered by an external excitation source signal such as an impulse hammer signal. The excitation and laser measurement signals are fed to a PC with an independent data logging ability.

The Polytec™ vibrometer software allows one to choose the data acquisition settings such as the sampling frequency, vibrometer sensitivity scale, filters, and window functions. The in-house data logging software is used to process the measured signals. This software has the capability to log time series, calculate spectra, and perform modal analysis and curve fitting to extract natural frequencies and mode shapes.

5.2 Results and Discussions. Results from the initial testing on the "undamped beam," that is, without the damping mechanism, showed that damping is extremely light. This ensures that the significant part of the damping comes from the localized con-

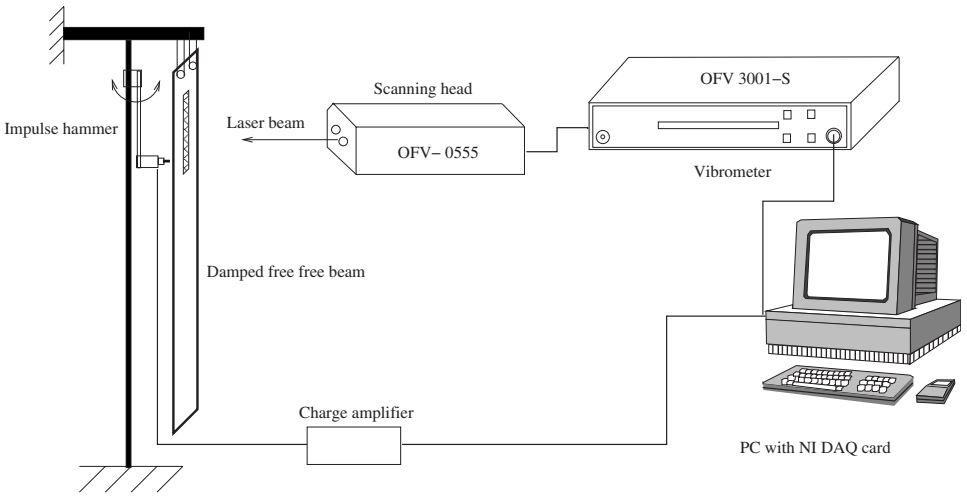

Fig. 1 Schematic representation of the experimental setup of the free-free beam

strained damping layer only. Measured natural frequencies, damping factors, and natural frequencies obtained from the FE method for the first 11 modes are shown in Table 2.

Timoshenko bending beam elements were used for the FE model. The degrees-of-freedom of the FE model (N) used in this study is 90, and the associated FE mesh is shown in Fig. 2. The schematic diagram of the FE mesh of the beam is shown in Fig. 2.

Percentage errors in the natural frequencies obtained from the finite element method with respect to the experimental methods are also shown in Table 2.

From the first two columns of this table, we fit a continuous function. Figure 3, shows the variation of modal damping factors for the first 11 modes.

Looking at the pattern of the curve in Fig. 3 we have selected the function $\hat{f}(\bullet)$ as

$$\zeta = \hat{f}(\omega) = a_0 + (a_1\omega^{-1} + a_2\omega^{-2} + a_3\omega^{-3}) + a_4 \exp\{-a_5(\omega - a_6)^2\} \tag{33}$$

where $a_i, i=1,\ldots,6$, are undetermined constants. Using the data in Table 2, together with a nonlinear least-squares error minimization approach, the fitted parameters are found to be.

$$a_0 = 0.0031, \quad a_1 = -6.26, \quad a_2 = 4.01 \times 10^3, \quad a_3 = -5.18 \times 10^5$$

$$a_4 = 0.0079, \quad a_5 = 6.96 \times 10^{-7}, \quad \text{and } a_6 = 8.4 \times 10^3 \tag{34}$$

Recalculated values of ζ_j using this fitted function is compared with the original function in Fig. 3. This function (the dotted line) matches well with the original modal data. We have also plotted the $\hat{f}(\omega)$ in Eq. (33) as functions of the natural frequencies from the experimental measurement and FE in Fig. 3. Both plots are reasonably close because the difference between the measured and FE natural frequencies is small in this case. Note that neither the function in Eq. (33) nor the parameter values in Eq. (34) are unique. One can use more complex functions and sophisticated parameter fitting procedures to obtain more accurate results.

Now that the function $\hat{f}(\omega)$ has been identified, the next step is

Table 2 Measured natural frequencies, damping factors, and natural frequencies obtained from the finite element (FE) method of the free-free beam for the first 11 modes (the numbers in the parentheses correspond to the percentage error with respect to the experimental result)

Natural frequencies, Hz (experimental)	Damping factors (in % of critical damping)	Natural frequencies, Hz (from FE)
33.00	0.6250	30.81 (−6.64%)
85.00	0.2000	85.24 (0.29%)
166.00	0.0833	167.61 (0.97%)
276.00	0.0313	277.73 (0.63%)
409.00	0.0625	415.67 (1.63%)
569.00	0.1250	581.42 (2.18%)
758.00	0.1163	774.94 (2.24%)
976.00	0.1786	996.20 (2.07%)
1217.00	0.8621	1245.15 (2.31%)
1498.00	0.7143	1521.77 (1.59%)
1750.00	0.3571	1826.06 (4.35%)

Fig. 2 Schematic representation of the finite element mesh of the of the free-free beam shown in Fig. 1

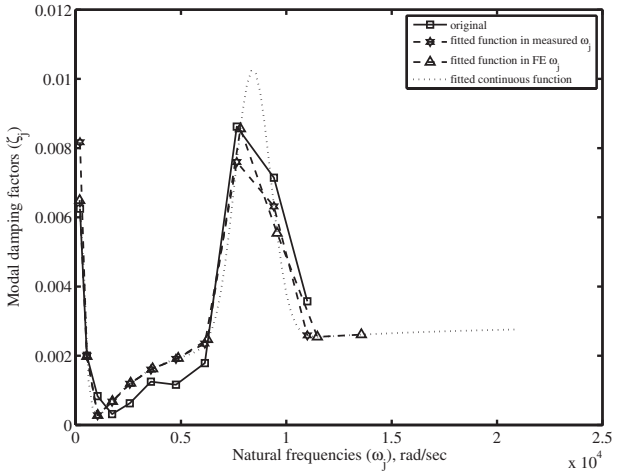

Fig. 3 Modal damping factors and fitted generalized proportional damping function for the first 11 modes

to substitute the 90×90 FE mass and stiffness matrices in Eq. (25) (or, equivalently, in Eq. (27)) to obtain the damping matrix. For this example we have

$$\hat{\mathbf{C}} = 2\mathbf{MT}[a_0\mathbf{I} + (a_1\mathbf{T}^{-1} + a_2\mathbf{T}^{-2} + a_3\mathbf{T}^{-3}) + a_4\exp\{-a_5(\mathbf{T} - a_6\mathbf{I})^2\}] \in \mathbb{R}^{90\times90} = 2(a_1\mathbf{M} + a_3\mathbf{K}) + 2\mathbf{M}\sqrt{\mathbf{M}^{-1}\mathbf{K}}[a_0\mathbf{I} + a_2\mathbf{K}^{-1}\mathbf{M} + a_4\exp\{-a_5(\sqrt{\mathbf{M}^{-1}\mathbf{K}} - a_6\mathbf{I})^2\}] \tag{35}$$

Interestingly, the first part of the $\hat{\mathbf{C}}$ matrix in Eq. (35) is the classical Rayleigh damping, while the second part is mass proportional in the sense of generalized proportional damping. The second part can be viewed as the correction needed to the Rayleigh damping model for the measured data set. Here we have compared our damping identification method with the following four methods:

(a) *Inverse modal transformation method*: This is a simple, yet very general, method to obtain the proportional damping matrix. Adhikari and Woodhouse [24] also used this approach in the context of identification of nonproportionally damped systems. From experimentally obtained modal damping factors and natural frequencies, one can construct the diagonal modal damping matrix $\mathbf{C}' = \mathbf{\Phi}^T\mathbf{C}\mathbf{\Phi}$ as

$$\mathbf{C}' = 2\boldsymbol{\zeta}\boldsymbol{\Omega} \tag{36}$$

From this, the damping matrix in the original coordinate can be obtained using the inverse transformation as

$$\hat{\mathbf{C}} = \mathbf{\Phi}^{-T}\mathbf{C}'\mathbf{\Phi}^{-1} \tag{37}$$

For a given structure, if the degrees-of-freedom of the FE model and experimental model (that is, the number of sensors and actuators) are the same, Eq. (37) and the proposed method would yield similar damping matrices. Usually the numerical model of a structure has more degrees-of-freedom compared to the degrees-of-freedom of the experimental model. Suppose that the numerical model has a dimension N and we have measured the modal parameters of first $n<N$ number of modes. The dimension of $\mathbf{C}'$ in Eq. (36) will be $n\times n$, whereas for further numerical analysis using the FE method we need the $\mathbf{C}$ matrix to be of the dimension $N\times N$. This implies that there is a need to extrapolate the available information. If the modal matrix from a FE model is used, one way this can be achieved is by using a $N\times n$ rectangular $\hat{\mathbf{\Phi}}$ matrix in Eq. (37), where the n columns of $\hat{\mathbf{\Phi}}$ would consist of the mode shapes corresponding to the measured modes. Since $\hat{\mathbf{\Phi}}$ becomes a rectangular matrix, a pseudo-inverse is required to calculate $\hat{\mathbf{\Phi}}^{-T}$ and $\hat{\mathbf{\Phi}}^{-1}$ in Eq. (37). Using the pseudo-inverse, the identified damping matrix can be obtained using Eq. (37) as

$$\hat{\mathbf{C}} = [(\hat{\mathbf{\Phi}}^T\hat{\mathbf{\Phi}})^{-1}\hat{\mathbf{\Phi}}^T]^T[2\boldsymbol{\zeta}\boldsymbol{\Omega}][(\hat{\mathbf{\Phi}}^T\hat{\mathbf{\Phi}})^{-1}\hat{\mathbf{\Phi}}^T] \tag{38}$$

(b) *Rayleigh's proportional damping method*: This is perhaps the most widely used approach for damping identification. The constants α_1 and α_2 can be obtained by an error minimization (least-squares for example) approach using Eq. (11). Once α_1 and α_2 are obtained, the damping matrix can be calculated using Eq. (6).

(c) *Caughey series method*: Géradin and Rixen [49] outlined a systematic method to obtain the damping matrix using the Caughey series (Eq. (7)). The coefficients α_j in series (7) can be obtained by solving the linear system of equations

$$\mathbf{W}\boldsymbol{\alpha} = \boldsymbol{\zeta}_v \tag{39}$$

where

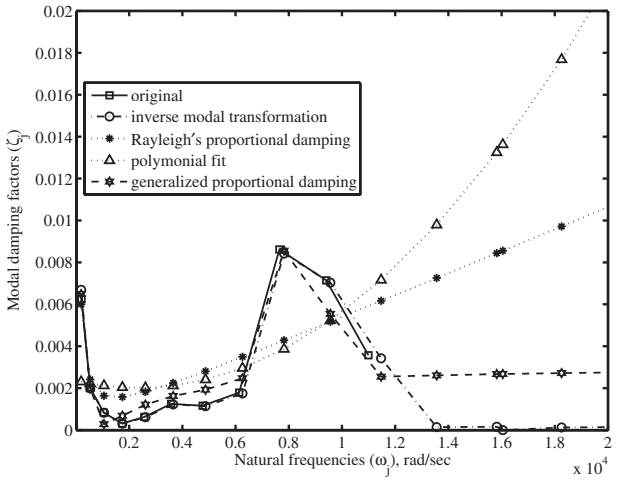

Fig. 4 Comparison of modal damping factors using different proportional damping matrix identification methods

$$\mathbf{W} = \frac{1}{2}\begin{bmatrix} \frac{1}{\omega_1} & \omega_1 & \omega_1^3 & \cdots & \omega_1^{2N-3} \\ \frac{1}{\omega_2} & \omega_2 & \omega_2^3 & \cdots & \omega_2^{2N-3} \\ \vdots & \vdots & \vdots & & \vdots \\ \frac{1}{\omega_N} & \omega_N & \omega_N^3 & \cdots & \omega_N^{2N-3} \end{bmatrix},$$

$$\boldsymbol{\alpha} = \begin{Bmatrix} \alpha_1 \\ \alpha_2 \\ \vdots \\ \alpha_N \end{Bmatrix}, \quad \text{and} \quad \boldsymbol{\zeta}_v = \begin{Bmatrix} \zeta_1 \\ \zeta_2 \\ \vdots \\ \zeta_N \end{Bmatrix} \tag{40}$$

The mass and stiffness matrices and the constants α_j calculated from the preceding equation can be substituted in Eq. (7) to obtain the damping matrix. Géradin and Rixen [49] mentioned that the coefficient matrix $\mathbf{W}$ in Eq. (40) becomes ill conditioned for systems with well separated natural frequencies.

(d) *Polynomial fit method*: In the Caughey series method, the coefficient matrix $\mathbf{W}$ in Eq. (40) becomes highly ill conditioned for systems with well separated natural frequencies. Therefore, a polynomial a of lower degree may be fitted to avoid the ill conditioning problem. The reconstructed damping matrix will have a similar form to the Caughey series except that it will be truncated.

The modal damping factors obtained using the proposed generalized proportional damping matrix in Eq. (35) is shown in Fig. 4.

In the same plot the results obtained from the other methods are also shown. In order to apply the inverse modal transformation method, only the first 11 columns of the analytical modal matrix are retained to obtain the truncated modal matrix $\hat{\mathbf{\Phi}} \in \mathbb{R}^{90\times11}$. This approach reproduces the damping factors for the first 11 modes very accurately. However, beyond the first 11 modes the damping factors obtained using the inverse modal transformation method is just zero (that is, effectively all the modes become undamped). The best fitted Rayleigh damping matrix for this example is obtained as

$$\hat{\mathbf{C}}_b = 2.28\mathbf{M} + 1.06\times10^{-6}\mathbf{K} \tag{41}$$

It was not possible to obtain the constants α_j from Eq. (39) using the Caughey method because the associated $\mathbf{W}$ matrix became highly ill conditioned. For the polynomial fit method, only a

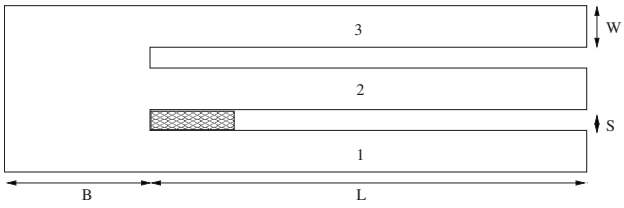

Fig. 5 Geometric parameters of the plate with slots: *B* =50 mm, *L*=400 mm, *S*=10 mm, and *W*=20 mm. The source of damping in this test structure is the wedged foam between beams 1 and 2.

second-order polynomial could be fitted to avoid the ill-conditioning problem. The best fitted second-order polynomial in this case turns out to be

$$\zeta = p_1 + p_2\omega + p_3\omega^2 \tag{42}$$

where

$$p_1 = 0.00236, \quad p_2 = -2.93 \times 10^{-7}, \quad \text{and } p_3 = 6.2 \times 10^{-11} \tag{43}$$

The damping matrix corresponding to the polynomial in Eq. (42) can be obtained as

$$\hat{\mathbf{C}}_d = 2\mathbf{MT}[p_1\mathbf{I} + p_2\mathbf{T} + p_3\mathbf{T}^2] = 2p_2\mathbf{K} + 2(p_1\mathbf{M} + p_3\mathbf{K})\sqrt{\mathbf{M}^{-1}\mathbf{K}} \tag{44}$$

This matrix, like the Rayleigh damping matrix, shows high modal damping values beyond the fitted modes.

6 Damping Identification in a Clamped Plate With Slots

6.1 System Model and Experimental Methodology. In this section we consider a two-dimensional structure. A schematic model of the test structure is shown in Fig. 5. This is fabricated by making slots in a mild steel rectangular plate of 2 mm thickness, resulting in three-cantilever beams joined at their base by a rectangular plate.

A schematic diagram of the test rig is shown in Fig. 6. The test system is fixed to a heavy table at the root so that the three-cantilever-like vanes are free to oscillate. A pendulum type impulse hammer is used to excite each vane of the structure close to the base of each vane. This mechanism delivers the impulse exactly at the same point repeatedly, so that better measurements can be obtained.

The data flow in the experiments is as follows. The impulse hammer signal is passed through a charge amplifier and then fed to the PC data logging system. The vibration response measured by the vibrometer is also fed to the PC to compute the frequency response function (FRF). The frequency response of this system shown in Fig. 7 exhibits a characteristic clustering of vibration modes into bands [4]. Notice that the coherence is very close to unity (zero on log scale) until 500 Hz, and the data of interest are in the range of 10–300 Hz. Thus a good FRF for each input/output combination was obtained. Also the peaks in each pass band are identifiable. Hence modal identification methods can be applied with ease on this data. The mode shapes for the three modes in the second and third bands are as shown in Figs. 8 and 9, respectively.

It can be seen that in the second pass band the cantilever beams deform in the second mode and that in the third pass band they deform in the third mode. Thus the approximate mode shapes in each pass band are [1 1 1], [1 0 −1], and [1 −2 1] based on a particular mode of single cantilever. Furthermore, by *suitably* varying the geometric parameters such as *B*, *L*, *S*, and *W* in Fig. 5, the modal overlap in each pass band can be controlled.

6.2 Results and Discussions. The finite element mesh of the test structure is shown in Fig. 10.

Measured natural frequencies, damping factors, and natural frequencies obtained from the FE method for the first nine modes are shown in Table 3.

Four noded rectangular plate bending elements were used for the FE model using the ABAQUS/standard software (Hibbit, Kralson & Soresen, Inc., Providence, RI). The resulting system model has 972 degrees of freedom. Percentage errors in the natural frequencies obtained from the finite element method with respect to the experimental methods are also shown in this table.

From the first two columns of Table 3, we fit a continuous function. Figure 11 shows the variation of modal damping factors for the first nine modes.

Looking at the pattern of the curve in Fig. 11, we have selected the function $\hat{f}(\bullet)$ as

$$\zeta = \hat{f}(\omega) = a_0 + a_1 \exp\{-a_2(\omega - a_3)^2\} + a_4 \exp\{-a_5(\omega - a_6)^2\} \tag{45}$$

where $a_i, i=0,\ldots,6$ are undetermined constants. Using the data in Table 3, together with a nonlinear least-squares error minimization approach, results in

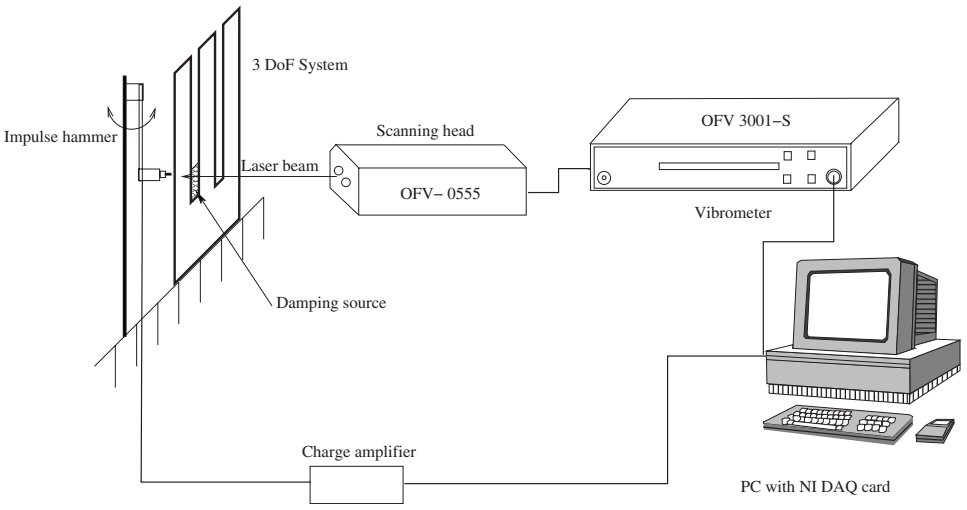

Fig. 6 Schematic representation of the experimental setup of the clamped plate with slots

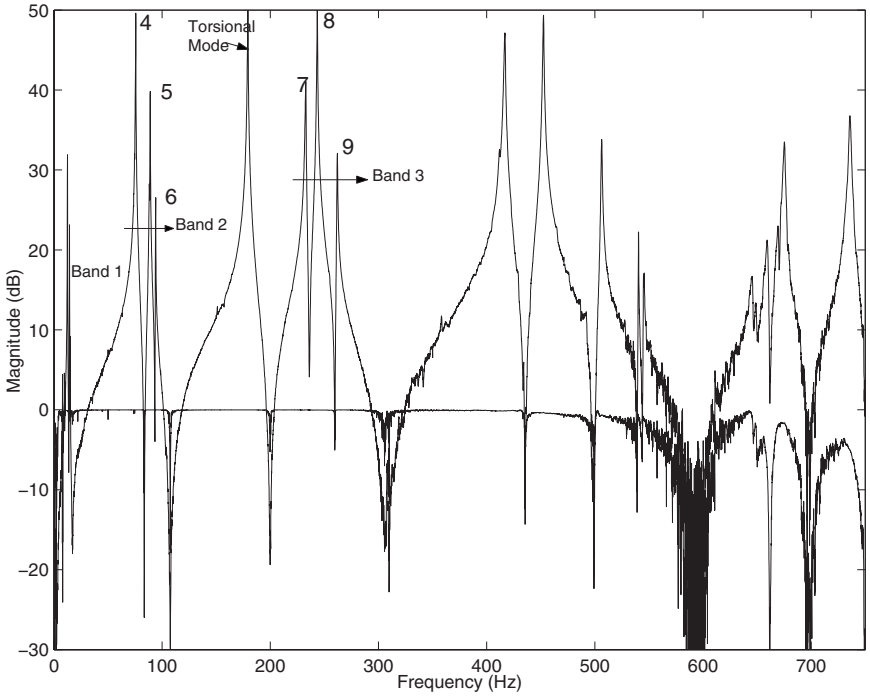

Fig. 7 Typical measured FRF on the three-cantilever system. Coherence is also shown on the same plot. Each pass band and flexural modes are labeled. Note that the peaks are clearly visible; hence modal identification can be performed with ease.

$$a_0 = 9.53 \times 10^{-4}, \quad a_1 = 4.51 \times 10^{-4}, \quad a_2 = 2.27 \times 10^{-5},$$

$$a_3 = 475$$

$$a_4 = 5.41 \times 10^{-4}, \quad a_5 = 3.7 \times 10^{-6}, \quad \text{and } a_6 = 1.46 \times 10^{3} \tag{46}$$

Recalculated values of ζ_j using this fitted function are compared with the original function in Fig. 11. This function (the dotted line) matches well with the original modal data. We have also plotted the $\hat{f}(\omega)$ in Eq. (33) as a function of the natural frequencies from the experimental measurement and FE in Fig. 11. Both plots are reasonably close because the difference between the measured

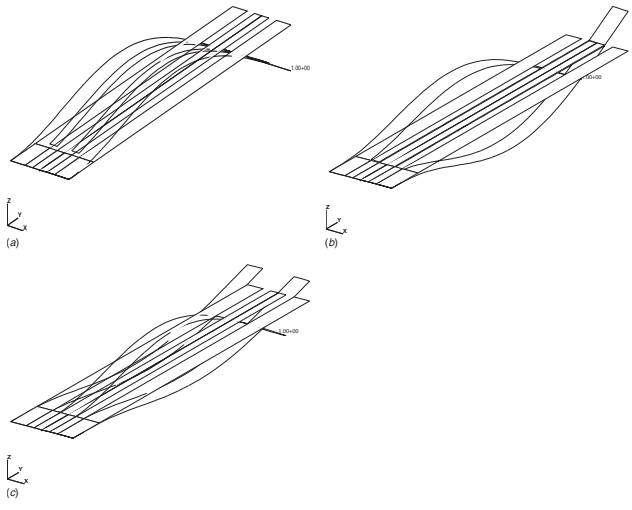

Fig. 8 Mode shapes corresponding to the three modes in the second pass band. It can be noticed that each of the cantilever beams deforms in its second mode in this band. Also notice that the second beam does not deform at all in the second mode of the pass band; i.e., it is a node. (*a*) Mode 1, (1, 1, 1); (*b*) Mode 2, (1, 0, –1); (*c*) Mode 3, (1, –2, 1).

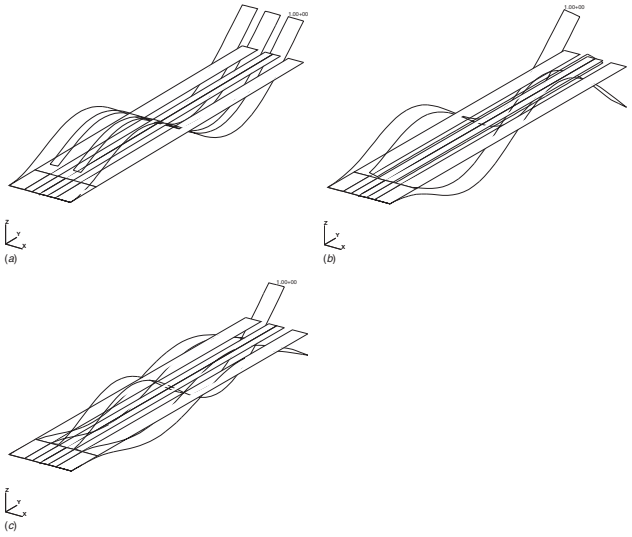

Fig. 9 Mode shapes corresponding to the three modes in the third pass band. It can be noticed that each of the cantilever beams deforms in its third mode in this band. Also notice that the second beam does not deform at all in the second mode of the pass band; i.e., it is a node. (*a*) Mode 1, (1, 1, 1); (*b*) Mode 2, (1, 0, –1); (*c*) Mode 3, (1, –2, 1).

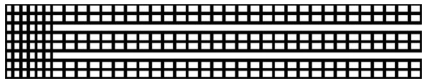

Fig. 10 Schematic representation of the finite element mesh of the clamped plate with slots shown in Fig. 6

Table 3 Measured natural frequencies, damping factors, and natural frequencies obtained from the FE method of the clamped plate with slots for the first nine modes (the numbers in the parentheses correspond to the percentage error with respect to the experimental result)

Natural frequencies, Hz (experimental)	Damping factors (in % of critical damping)	Natural frequencies, Hz (from FE)
12.46	0.1032	13.14 (5.44%)
14.36	0.0969	14.45 (0.65%)
15.01	0.1159	15.08 (0.45%)
75.60	0.1404	81.32 (7.56%)
88.94	0.1389	89.68 (0.83%)
93.97	0.1254	94.49 (0.55%)
232.74	0.1494	225.95 (−2.92%)
243.37	0.0953	248.53 (2.12%)
261.93	0.1260	265.04 (1.19%)

and FE natural frequencies is small in this case. Again, neither the function in Eq. (45) nor the parameter values in Eq. (46) are unique. One can use more complex functions and sophisticated parameter fitting procedures to obtain more accurate results.

After the identification of the function $\hat{f}(\omega)$, the next step is to substitute the 972×972 FE mass and stiffness matrices in Eq. (25) (or, equivalently, in Eq. (27)) to obtain the damping matrix. For this example we have

$$\hat{\mathbf{C}} = 2\mathbf{MT}[a_0\mathbf{I} + a_1\exp\{-a_2(\mathbf{T}-a_3\mathbf{I})^2\} + a_4\exp\{-a_5(\mathbf{T}-a_6\mathbf{I})^2\}] \in \mathbb{R}^{972\times972} \tag{47}$$

Again we have compared our damping identification method with the other four methods discussed before. The modal damping factors obtained using the proposed generalized proportional damping matrix in Eq. (47) are shown in Fig. 12.

In the same plot the results obtained from the other methods are also shown. In order to apply the inverse modal transformation method, only the first nine columns of the analytical modal matrix are retained to obtain the truncated modal matrix $\hat{\mathbf{\Phi}} \in \mathbb{R}^{972\times9}$. This approach reproduces the damping factors for the first nine modes very accurately. However, beyond the first nine modes, the damping factors obtained using the inverse modal transformation

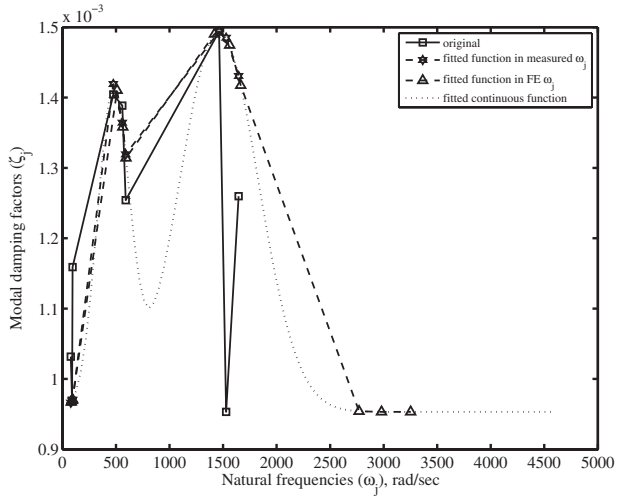

Fig. 11 Modal damping factors and fitted generalized proportional damping function for the first nine modes of the clamped plate with slots

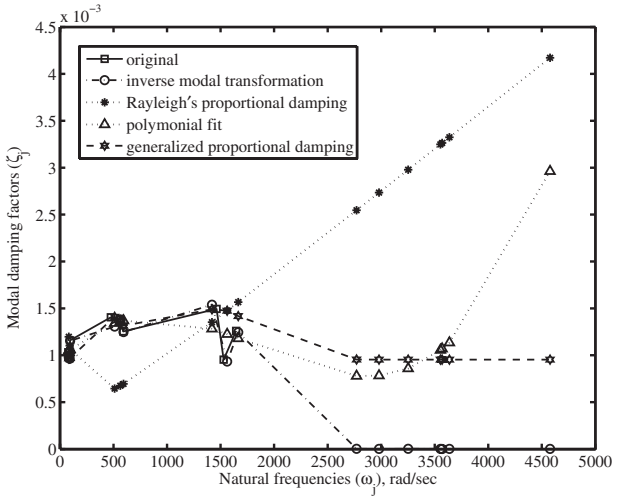

Fig. 12 Comparison of modal damping factors using different proportional damping matrix identification methods for the clamped plate with slots

method is just zero (that is, effectively all the modes become undamped). The best fitted Rayleigh damping matrix for this example is obtained as

$$\hat{\mathbf{C}}_b = 0.185\mathbf{M} + 1.81\times10^{-6}\mathbf{K} \tag{48}$$

It was not possible to obtain the constants α_j from Eq. (39) using the Caughey method because the associated $\mathbf{W}$ matrix became highly ill conditioned. For the polynomial fit method, only a third-order polynomial could be fitted to avoid the ill-conditioning problem. The best fitted third-order polynomial in this case turns out to be

$$\zeta = p_1 + p_2\omega + p_3\omega^2 + p_4\omega^3 \tag{49}$$

where

$$p_1 = 9.61\times10^{-4},\quad p_2 = 1.15\times10^{-6},\quad p_3 = -8.73\times10^{-10},\quad \text{and } p_3 = 1.57\times10^{-13} \tag{50}$$

The damping matrix corresponding to the polynomial in Eq. (49) can be obtained as

$$\hat{\mathbf{C}}_d = 2\mathbf{MT}[p_1\mathbf{I} + p_2\mathbf{T} + p_3\mathbf{T}^2 + p_4\mathbf{T}^3] = 2p_2\mathbf{K} + 2(p_1\mathbf{M} + p_3\mathbf{K})\sqrt{\mathbf{M}^{-1}\mathbf{K}} + 2p_4\mathbf{K}\mathbf{M}^{-1}\mathbf{K} \tag{51}$$

This matrix, like the Rayleigh damping matrix, shows high modal damping values beyond the fitted modes.

7 Damping Identification in Point Coupled Beams

7.1 System Model and Experimental Methodology. In this section, experimental damping identification on a coupled one-dimensional structure will be described. The structure comprises two mild steel cantilevered beams of different lengths with point masses, coupled by a brass rod, as shown in Fig. 13. The physical parameters of each beam, the coupling rod and the point masses are as given in Table 4. The drive-point response at the point of coupling between two beams was measured for individual beams without coupling first and then on the coupled system using the impulse excitation technique. The FRFs are used to obtain the natural frequency and damping factors using the procedures described earlier in Sec. 5.

7.2 Results and Discussions. Timoshenko beam elements are used for the finite element model of the beams. Measured natural frequencies, damping factors, and natural frequencies obtained from the FE method for the top, bottom, and coupled beams are

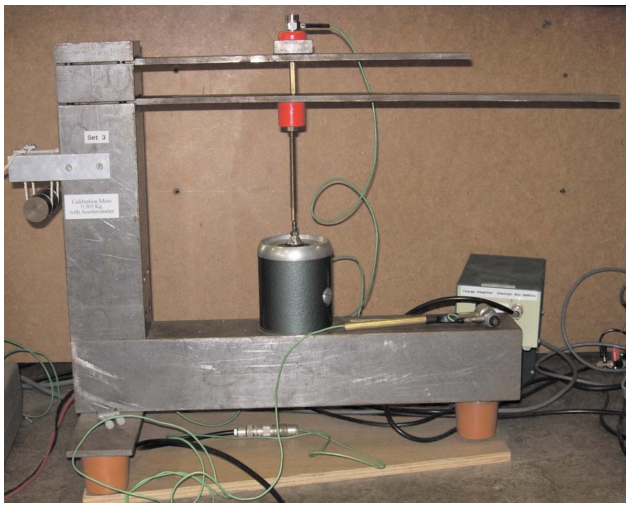

Fig. 13 Experimental setup for the point coupled beams. (Courtesy to Cambridge University Engineering Department for allowing using this figure.)

Table 5 Measured natural frequencies, damping factors, and natural frequencies obtained from the FE method of the top, bottom, and coupled beams (the numbers in the parentheses correspond to the percentage error with respect to the experimental result)

Natural frequencies, Hz (experimental)	Damping factors (in % of critical damping)	Natural frequencies, Hz (from FE)
Top beam		
44.00	0.2778	44.16 (0.37%)
235.00	0.4950	237.23 (0.95%)
Bottom beam		
23.00	0.4310	21.56 (−6.27%)
133.00	0.1718	135.11 (1.58%)
366.00	0.2439	378.43 (3.40%)
Coupled system		
28.00	1.6667	27.56 (−1.55%)
77.00	0.1923	79.57 (3.34%)
188.00	0.4065	186.52 (−0.79%)
322.00	0.2500	318.35 (−1.13%)

shown in Table 5.

The resulting model has 45 degrees of freedom for the top beam, 27 degrees of freedom for the top beam for the bottom beam, and 177 degrees of freedom for the coupled system. The schematic diagram of the FE mesh of the coupled beam system is shown in Fig. 14.

Percentage errors in the natural frequencies obtained from the finite element method with respect to the experimental methods are also shown in this table.

Figure 15 shows the variation of modal damping factors for the top beam, the bottom beam, and the coupled system.

From the first two columns of Table 5, we fit continuous functions corresponding to these variations. The following functions are selected for the three cases, respectively:

$$\text{Top beam:} \quad \zeta_t = \hat{f}_t(\omega) = a_0 + (a_1 + a_2\omega)\exp\{-a_3(\omega - a_4)^2\} \tag{52}$$

Table 4 Material and geometric properties of the coupled structure

Property	Numerical values
Top beam	
Length	330 mm
Width	51 mm
Thickness	63 mm
Young's modulus	210 GPa
Density	7840 kg m^{-3}
Point mass	0.182 kg
Bottom beam	
Length	483 mm
Width	51 mm
Thickness	63 mm
Young's modulus	210 GPa
Density	7840 kg m^{-3}
Coupling rod	
Length	32.5 mm
Diameter	3.5 mm
Young's modulus	105 GPa
Density	8210 kg m^{-3}

$$\text{Bottom beam:} \quad \zeta_b = \hat{f}_b(\omega) = b_0 + (b_1\omega^{-1} + b_2\omega^{-2} + b_3\omega^{-3}) \tag{53}$$

$$\text{Coupled system:} \quad \zeta_c = \hat{f}_c(\omega) = c_0 + (c_1\omega^{-1} + c_2\omega^{-2} + c_3\omega^{-3}) \tag{54}$$

where a_i, b_i, and c_i are undetermined constants. Using the data in Table 5, together with a nonlinear least-squares error minimization approach, results in

$$a_0 = 0.00386, \quad a_1 = -0.00158, \quad a_2 = 1.79 \times 10^{-6},$$

$$a_3 = 1.49 \times 10^3, \quad a_4 = 4.87 \times 10^{-7}$$

$$b_0 = 0.00282, \quad b_1 = -1.26, \quad b_2 = 282, \quad b_3 = -9.21 \times 10^3 \tag{55}$$

$$c_0 = 0.00629, \quad c_1 = -5.64, \quad c_2 = 2.02 \times 10^3, \quad \text{and}$$

$$c_3 = -1.27 \times 10^5$$

Recalculated values of ζ_j using these fitted functions are compared with the original functions in Fig. 15. These functions match well with the original modal data.

Now that the functions $\hat{f}(\omega)$ have been identified for the three cases, the next step is to substitute the respective FE mass and stiffness matrices in Eq. (25) (or, equivalently, in Eq. (27)) to obtain the damping matrix. For this example we have

$$\text{Top beam:} \quad \hat{\mathbf{C}}_t = 2\mathbf{M}_t\mathbf{T}_t[a_0\mathbf{I} + (a_1\mathbf{I} + a_2\mathbf{T}_t)\exp\{-a_3(\mathbf{T}_t - a_4\mathbf{I})^2\}] \in \mathbb{R}^{45\times 45} \tag{56}$$

$$\text{Bottom beam:} \quad \hat{\mathbf{C}}_b = 2\mathbf{M}_b\mathbf{T}_b[b_0\mathbf{I} + (b_1\mathbf{T}_b^{-1} + b_2\mathbf{T}_b^{-2} + b_3\mathbf{T}_b^{-3})] \in \mathbb{R}^{27\times 27} \tag{57}$$

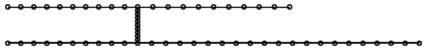

Fig. 14 Schematic representation of the finite element mesh of the of the coupled beam system shown in Fig. 13

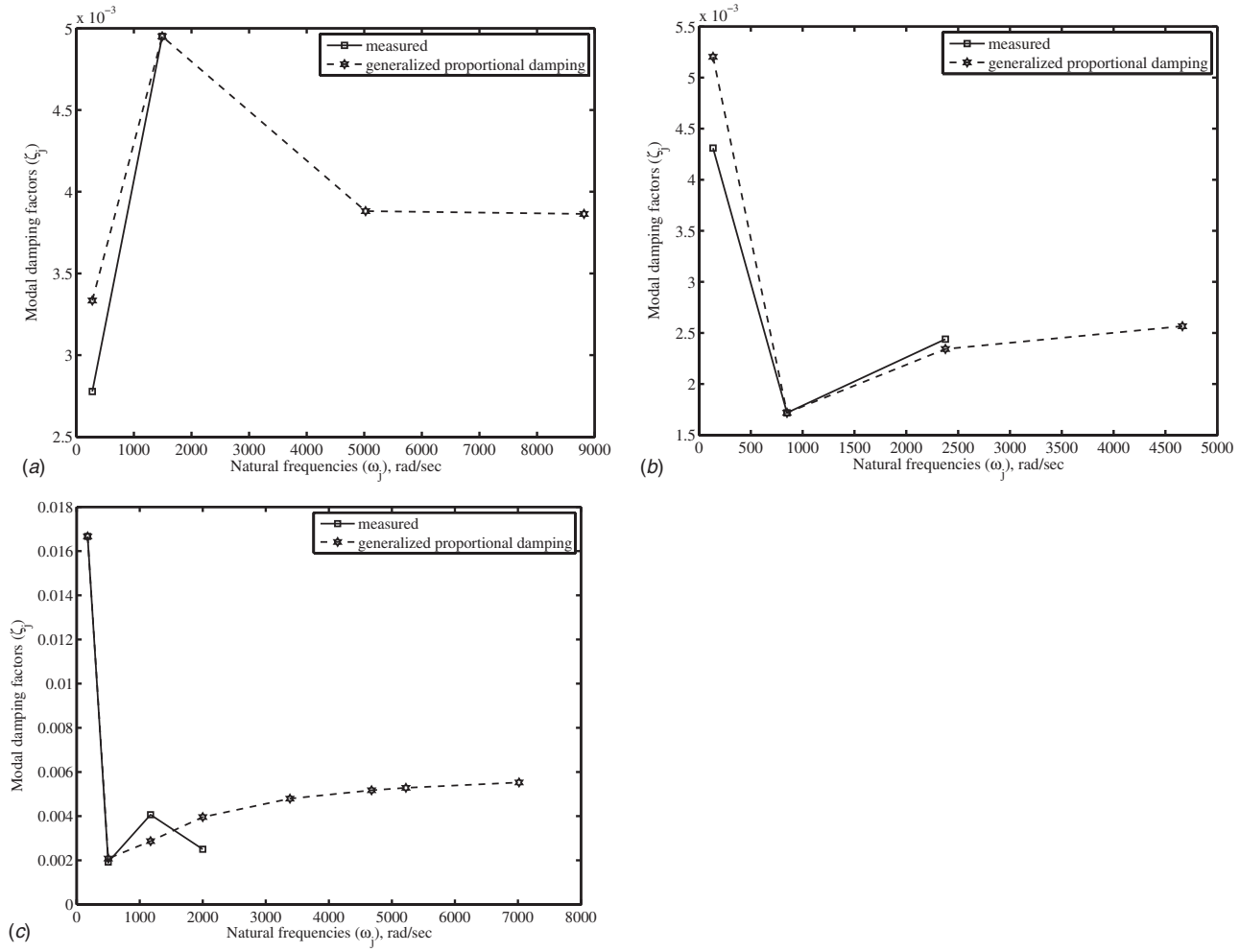

Fig. 15 Modal damping factors and fitted generalized proportional damping function for the coupled beam system. (*a*) Top beam; (*b*) bottom beam; (*c*) coupled system.

$$\text{Coupled system:} \quad \hat{\mathbf{C}}_c = 2\mathbf{M}_c\mathbf{T}_c[c_0\mathbf{I} + (c_1\mathbf{T}_c^{-1} + c_2\mathbf{T}_c^{-2} + c_3\mathbf{T}_c^{-3})] \in \mathbb{R}^{177\times 177} \tag{58}$$

For this example the damping factors of the coupled system were available. This allowed us to obtain the damping matrix of the coupled system using the generalized proportional damping. If the damping factors of the coupled system were not available, the corresponding damping matrix could have been obtained from the damping matrices corresponding to the top and bottom beams, respectively.

8 Conclusions

The damping matrix identification approach based on generalized proportional damping is considered in this paper. The generalized proportional damping expresses the damping matrix in terms of smooth continuous functions involving specially arranged mass and stiffness matrices so that the system still posseses classical normal modes. This enables one to model variations in the modal damping factors with respect to the frequency in a simplified manner. Once a scalar function is fitted to model such variations, the damping matrix can be identified very easily using the proposed method. This implies that the problem of damping identification is effectively reduced to the problem of a scalar function fitting. The method is simple and requires the measurement of damping factors and natural frequencies only. Closed-form expressions are derived for the error propagation in the damping identification method. The proposed method is applicable to any linear structures, provided that damping is not very high and the modes are not too close so that they can be assumed to be real. If a system is heavily damped and modes are highly complex, the proposed identified damping matrix can be a good starting point for more sophisticated analyses.

The damping matrix identification method was applied to three laboratory based examples involving a free-free beam, a plate with slots, and a system consisting of two coupled beams. For the first two examples, the proposed method was compared to existing methods such as the inverse modal transformation method, Rayleigh proportional damping method, Caughey series method, and polynomial fit method. The modal damping factors recalculated using the damping matrix obtained from the proposed generalized viscous damping method agree well with the measured damping factors. The proposed methodology is simple and sufficiently general to be applied in large-scale industrial structures.

Acknowledgment

S.A. acknowledges the support of the Engineering and Physical Sciences Research Council (EPSRC) through the award of an advanced research fellowship. A.S.P. acknowledges the support from Cambridge Commonwealth Trust through the award of Nehru Fellowship during the period of this work.

Nomenclature

α_1, α_2 = proportional damping constants

$\boldsymbol{\alpha}$ = a vector containing the constants in the Caughey series
$\mathbf{C}$ = viscous damping matrix
$\mathbf{f}(t)$ = applied dynamic loading
$\mathbf{K}$ = stiffness matrix
$\mathbf{M}$ = mass matrix
$\boldsymbol{\Omega}$ = diagonal matrix containing the natural frequencies
$\boldsymbol{\Phi}$ = undamped modal matrix
$\mathbf{q}(t)$ = dynamic response (generalized coordinates)
$\mathbf{T}$ = a temporary matrix, $\mathbf{T}=\sqrt{\mathbf{M}^{-1}\mathbf{K}}$
$\mathbf{W}$ = coefficient matrix associated with the constants in the Caughey series
$\boldsymbol{\zeta}$ = diagonal matrix containing the modal damping factors
$\boldsymbol{\zeta}_v$ = a vector containing the modal damping factors
ω_j = natural frequencies
$\hat{f}(\cdot)$ = fitted modal damping function
ζ_j = modal damping factors
$(\cdot)^T$ = matrix transpose
$(\cdot)^{-1}$ = matrix inverse
$(\cdot)^{-T}$ = matrix inverse transpose
$(\cdot)_{(e)}, (\cdot)^{(e)}$ = $(\cdot)$ of the eth element/substructure

References

[1] Nashif, A. D., Jones, D. I. G., and Henderson, J. P., 1985, *Vibration Damping*, 1st ed., Wiley, New York.
[2] Lazan, B., 1968, *Damping of Materials and Members in Structural Mechanics*, 1st ed., Pergamon, London.
[3] Ungar, E. E., 1973, "The Status of Engineering Knowledge Concerning the Damping of Built-Up Structures," J. Sound Vib., **26**(1), pp. 141–154.
[4] Phani, A. S., 2004, "Damping Identification in Linear Vibrations," Ph.D. thesis, Cambridge University Engineering Department, Trumpington Street, Cambridge, CB2 1PZ.
[5] Rayleigh, L., 1877, *Theory of Sound*, 2nd ed., Dover, New York.
[6] Ewins, D. J., 2000, *Modal Testing: Theory and Practice*, 2nd ed., Research Studies, Baldock, England.
[7] Maia, N. M. M., Silva, J. M. M., and Roberts, J. B., 1997, *Theoretical and Experimental Modal Analysis*, Engineering Dynamics Series, Research Studies, Taunton, England.
[8] Silva, J. M. M., and Maia, N. M. M., 1998, *Modal Analysis and Testing: Proceedings of the NATO Advanced Study Institute*, NATO Advanced Study Institute, Series E: Applied Science, Sesimbra, Portugal.
[9] Newland, D. E., 1987, "On the Modal Analysis of Nonconservative Linear Systems," J. Sound Vib., **112**(1), pp. 69–96.
[10] Newland, D. E., 1989, *Mechanical Vibration Analysis and Computation*, Wiley, New York.
[11] Bishop, R. E. D., and Johnson, D. C., 1960, *The Mechanics of Vibration*, Cambridge University Press, Cambridge, England.
[12] Caughey, T. K., and O'Kelly, M. E. J., 1965, "Classical Normal Modes in Damped Linear Dynamic Systems," ASME Trans. J. Appl. Mech., **32**, pp. 583–588.
[13] Adhikari, S., 2006, "Damping Modelling Using Generalized Proportional Damping," J. Sound Vib., **293**(1–2), pp. 156–170.
[14] Pilkey, D. P., and Inman, D. J., 1998, "Survey of Damping Matrix Identification," *Proceedings of the 16th International Modal Analysis Conference (IMAC)*, Santa Barbara, CA, February 1998, Vol. 1.
[15] Fabunmi, J., Chang, P., and Vorwald, J., 1988, "Damping Matrix Identification Using the Spectral Basis Technique," Trans. ASME, J. Vib., Acoust., Stress, Reliab. Des., **110**, pp. 332–337.
[16] Lancaster, P., 1961, "Expression of Damping Matrices in Linear Vibration Problems," J. Aerosp. Sci., **28**, p. 256.
[17] Hasselsman, T. K., 1972, "A Method of Constructing a Full Modal Damping Matrix From Experimental Measurements," AIAA J., **10**(4), pp. 526–527.
[18] Béliveau, J.-G., 1976, "Identification of Viscous Damping in Structures From Modal Information," ASME Trans. J. Appl. Mech., **43**, pp. 335–339.
[19] Ibrahim, S. R., 1983, "Dynamic Modeling of Structures From Measured Complex Modes," AIAA J., **21**(6), pp. 898–901.
[20] Minas, C., and Inman, D. J., 1991, "Identification of a Nonproportional Damping Matrix From Incomplete Modal Information," Trans. ASME, J. Vib. Acoust., **113**, pp. 219–224.
[21] Starek, L., and Inman, D. J., 1997, "A Symmetric Inverse Vibration Problem for Nonproportional Underdamped Systems," Trans. ASME, J. Appl. Mech., **64**, pp. 601–605.
[22] Pilkey, D. F., and Inman, D. J., 1997, "Iterative Approach to Viscous Damping Matrix Identification," *Proceedings of the 15th International Modal Analysis Conference (IMAC)*, Orlando, FL, February 1997, Vol. 2.
[23] Alvin, K. F., Peterson, L. D., and Park, K. C., 1997, "Extraction of Normal Modes and Full Modal Damping From Complex Modal Parameters," AIAA J., **35**(7), pp. 1187–1194.
[24] Adhikari, S., and Woodhouse, J., 2001, "Identification of Damping: Part 1, Viscous Damping," J. Sound Vib., **243**(1), pp. 43–61.
[25] Adhikari, S., and Woodhouse, J., 2001, "Identification of Damping: Part 2, Non-Viscous Damping," J. Sound Vib., **243**(1), pp. 63–88.
[26] Adhikari, S., and Woodhouse, J., 2002, "Identification of Damping: Part 3, Symmetry-Preserving Method," J. Sound Vib., **251**(3), pp. 477–490.
[27] Adhikari, S., and Woodhouse, J., 2002, "Identification of Damping: Part 4, Error Analysis," J. Sound Vib., **251**(3), pp. 491–504.
[28] Barbieri, N., de Souza, O. H., and Barbieri, R., 2004, "Dynamical Analysis of Transmission Line Cables. Part 2—Damping Estimation," Mech. Syst. Signal Process., **18**(3), pp. 671–681.
[29] Barbieri, N., Novak, P. R., and Barbieri, R., 2004, "Experimental Identification of Damping," Int. J. Solids Struct., **41**(13), pp. 3585–3594.
[30] Popov, A. A., and Geng, Z. M., 2005, "Modelling of Vibration Damping in Pneumatic Tyres," Veh. Syst. Dyn., **43**, pp. 145–155.
[31] Segalman, D. J., 2006, "Modelling Joint Friction in Structural Dynamics," Struct. Control Health Monit., **13**(1), pp. 430–453.
[32] Caravani, P., and Thomson, W. T., 1974, "Identification of Damping Coefficients in Multidimensional Linear Systems," ASME Trans. J. Appl. Mech., **41**, pp. 379–382.
[33] Fritzen, C.-P., 1986, "Identification of Mass, Damping and Stiffness Matrices of Mechanical Systems," Trans. ASME, J. Vib., Acoust., Stress, Reliab. Des., **108**, pp. 9–16.
[34] Mottershead, J. E., 1990, "Theory for the Estimation of Structural Vibration Parameters From Incomplete Data," AIAA J., **28**(3), pp. 559–561.
[35] Roemer, M. J., and Mook, D. J., 1992, "Mass, Stiffness and Damping Matrix Identification: An Integrated Approach," Trans. ASME, J. Vib. Acoust., **114**, pp. 358–363.
[36] Chen, S. Y., Ju, M. S., and Tsuei, Y. G., 1996, "Estimation of Mass Stiffness and Damping Matrices From Frequency Response Function," Trans. ASME, J. Vib. Acoust., **118**, pp. 78–82.
[37] Baruch, M., 1997, "Identification of the Damping Matrix," TAE Technical Report No. 803, Technion, Israel, Faculty of Aerospace Engineering, Israel Institute of Technology, Haifa.
[38] Adhikari, S., 2002, "Lancaster's Method of Damping Identification Revisited," Trans. ASME, J. Vib. Acoust., **124**(4), pp. 617–627.
[39] Khalil, M., Adhikari, S., and Sarkar, A., 2007, "Linear System Identification Using Proper Orthogonal Decomposition," Mech. Syst. Signal Process., **21**(8), pp. 3123–3145.
[40] Phani, A. S., and Woodhouse, J., "Viscous Damping Identification in Linear Vibration," J. Sound Vib., **303**, (3–5), pp. 475–500.
[41] Imregun, M., and Ewins, D. J., 1995, "Complex Modes: Origin and Limits," *Proceedings of the 13th International Modal Analysis Conference (IMAC)*, Nashville, TN, February 1995.
[42] Adhikari, S., 2004, "Optimal Complex Modes and an Index of Damping Non-Proportionality," Mech. Syst. Signal Process., **18**(1), pp. 1–27.
[43] Phani, A. S., 2003, "On the Necessary and Sufficient Conditions for the Existence of Classical Normal Modes in Damped Linear Dynamic Systems," J. Sound Vib., **264**(3), pp. 741–745.
[44] Bellman, R., 1960, *Introduction to Matrix Analysis*, McGraw-Hill, New York.
[45] Allemang, R. J., and Brown, D. L., 1982, "A Correlation Coefficient for Modal Vector Analysis," *Proceedings of the First International Modal Analysis Conference (IMAC)*, Orlando, FL.
[46] Friswell, M. I., and Mottershead, J. E., 1995, *Finite Element Model Updating in Structural Dynamics*, Kluwer Academic, The Netherlands.
[47] Harville, D. A., 1998, *Matrix Algebra From a Statistician's Perspective*, Springer-Verlag, New York.
[48] Ungar, E. E., 2000, "Damping by Viscoelastic Layers," Appl. Mech. Rev., **53**(6), pp. R33–R38.
[49] Géradin, M., and Rixen, D., 1997, *Mechanical Vibrations*, 2nd ed., Wiley, New York.